Numerical simulation of shear wall failure mechanisms

F. Dashti, R.P. Dhakal & S. Pampanin

Department of Civil and Natural Resources Engineering, University of Canterbury, Christchurch, New Zealand

2014 NZSEE Conference

ABSTRACT: This study investigates the ability of a finite element model in predicting nonlinear behavior and failure patterns of RC structural walls. Experimental results of walls with different shear-span ratios which failed in different modes are used for verification. The walls are modelled in the finite element analysis program DIANA9.4.4. Curved shell elements with embedded bar elements are used to simulate the reinforced concrete section of the walls to be analysed. This type of model does not require 'plane sections to remain plane' along a wall, and simulates the in-plane axial-flexure-shear interaction without requiring any empirical adjustment. The model is found to capture the monotonic and cyclic responses of the tested wall specimens with reasonable accuracy in terms of hysteresis curves and failure patterns. The failure patterns simulated by the model include shear, flexure, flexure-shear and flexure-out of plane modes depending on different parameters particularly shear-span ratio of the specimens. Moreover, the strain profile captured by the model was in good agreement with experimental measurements indicating that in addition to the overall global response predictions, local behaviour of the wall models can be predicted reasonably well.

1 INTRODUCTION

Structural walls (also known as shear walls) are one of the common lateral load resisting elements in reinforced concrete (RC) buildings in seismic regions. According to Canterbury Earthquakes Royal Commission Reports (2012), structural walls in Christchurch buildings did not perform as anticipated. Boundary zone crushing and bar buckling were observed in most pre-1970s RC walls which were generally lightly reinforced, were not detailed for ductility and had inadequate reinforcement to provide confinement to the concrete and buckling restraint to the longitudinal reinforcement. On the other hand, modern (post-1970s) RC wall buildings were observed to have experienced failure patterns like wall web buckling, boundary zone bar fracture and buckling failure of ducted splice. In a number of cases, compression failure occurred in the outstanding legs of T and L walls in addition to out-of-plane displacements, thereby resulting in overall buckling of the wall. In some cases, transverse reinforcement did not meet the spacing requirement to prevent buckling of the longitudinal reinforcement, and bar buckling resulted in high localized strains and decreased the tensile strain capacity. Figure 1a summarizes the key statistics and findings from the processed Building Safety Evaluation (BSE) building database and Figure 1b shows damage statistics of 44 shear wall buildings in the Christchurch Central Business District (CCBD).

As shown in Figure 1a, 23% of the 40 buildings were built before 1970's and were not designed with capacity design concept. Nevertheless, some of these pre-1970's buildings performed satisfactorily in the earthquakes due to significant structural redundancy with larger shear wall widths. Over 70% of the 40 wall buildings were post-1970's structures, yet they sustained severe damage from brittle shear-compression, premature reinforcing tensile or compressive fracture failure mechanisms, due to high level of axial load, compression–shear interaction, bidirectional loading, high slenderness or aspect ratio, low amount of longitudinal reinforcement ratio, and inadequate confinement detailing. According to Figure 1b, about 30% of the RC wall buildings built between 1990s and 2010s were assessed as "Red - Unsafe"; while only 15% of the pre-1970s RC wall buildings were red-tagged.

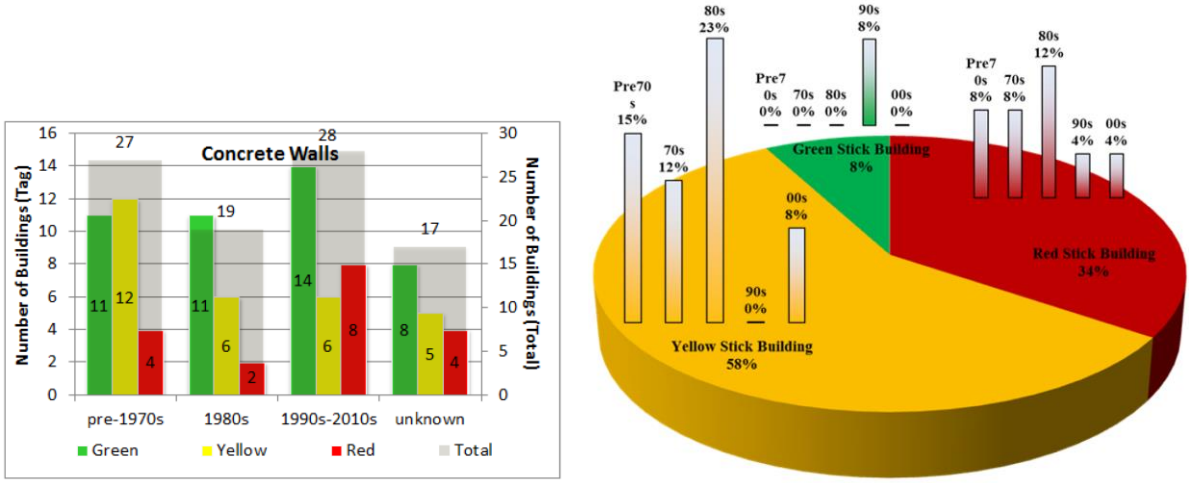

a) b)

Figure 1. Wall failure statistics in the recent Christchurch earthquakes: a) Distribution of Building Safety Evaluation placards of all buildings in the Christchurch CBD (Kam et al. 2011), b) Damages statistics of 44 shear wall buildings in CCBD (Park and Chen 2012).

Figure 2 and Figure 3 show some examples of different failure modes, observed in RC walls in 2011 Christchurch earthquake. As a result of the unexpected performance of shear walls in recent earthquakes in New Zealand, some issues have been identified to be further investigated (NZRC 2012). The main issues lie around the buckling of bars, out-of plane deformation of the wall (especially the zone deteriorated in compression), reinforcement getting snapped beneath a solitary thin crack etc.

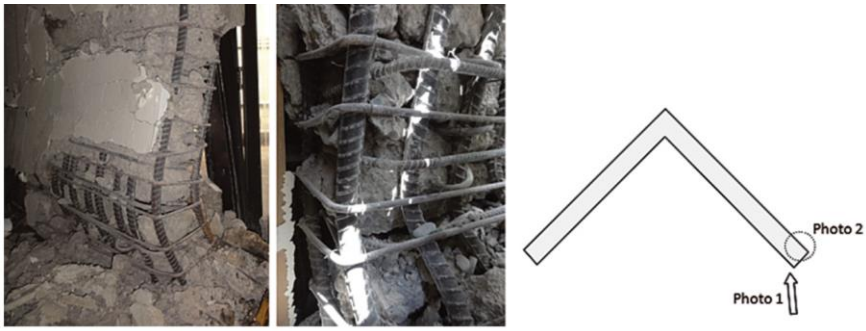

Figure 2. Web buckling of well-confined wall (Elwood 2013)

The performance of RC structural walls in recent earthquakes has exposed some problems with the existing design of RC structural walls; leading to a call for the wall design procedures to be reviewed and improved. Before design guidelines can be improved, it is necessary to investigate the nonlinear seismic response of walls including the causes of different failure modes observed in the recent earthquakes. As repeated experimental investigation is too demanding, a more plausible way to scrutinize the observed performance of RC shear walls against their expected performance is simulating the walls using an efficient analytical model.

a) b)

Figure 3: a) Bar buckling and fracture in lightly reinforced slender RC shear wall

b) Slender wall shear-axial failure (Kam et al. 2011)

This study investigates the ability and robustness of a finite element model in predicting nonlinear behavior and failure patterns of walls. Experimental results of walls with different shear-span ratios which failed in different modes are used for the verification of the model.

2 MODEL DESCRIPTION

Two dimensional nonlinear finite element analyses were carried out on RC shear walls subjected to monotonic and cyclic in-plane lateral loadings using DIANA9.4.4 (DIANA 2011). Curved shell elements with embedded bar elements were used to simulate the RC walls. The curved shell elements in DIANA (Figure 4a) are based on isoparametric degenerated solid approach by introducing two shell hypotheses (DIANA 2011):

Straight-normals: Assumes that normals remain straight, but not necessarily normal to the reference surface. Transverse shear deformation is included according to the Mindlin-Reissner theory.

Zero-normal-stress: Assumes that the normal stress component in the normal direction of a lamina basis is forced to zero: $\sigma_{zzl(\xi,\eta,z)} = 0$. The element tangent plane is spanned by a lamina basis which corresponds to a local Cartesian coordinate system (x_l, y_l) defined at each point of the shell with x_l and y_l tangent to the ξ, η plane and z_l perpendicular to it.

The in-plane lamina strains ε_{xx}, ε_{yy} and γ_{xy} vary linearly in the thickness direction. The transverse shear strains γ_{xz} and γ_{yz} are forced to be constant in the thickness direction. Since the actual transverse shearing stresses and strains vary parabolically over the thickness, the shearing strains are an equivalent constant strain on a corresponding area. A shear correction factor is applied using the condition that a constant transverse shear stress yields approximately the same shear strain energy as the actual shearing stress.

Five degrees of freedom have been defined in every element node: three translations and two rotations. Further characteristics of curved shells are the following. They must be thin, i.e., the thickness ‘t’ must be small in relation to the dimensions b in the plane of the element. Force loads ‘F’ may act in any direction between perpendicular to the surface and in the surface. Moment loads ‘M’ should act around an axis which is in the element face. A typical finite element model is shown for one of the specimens in Figure 4b.

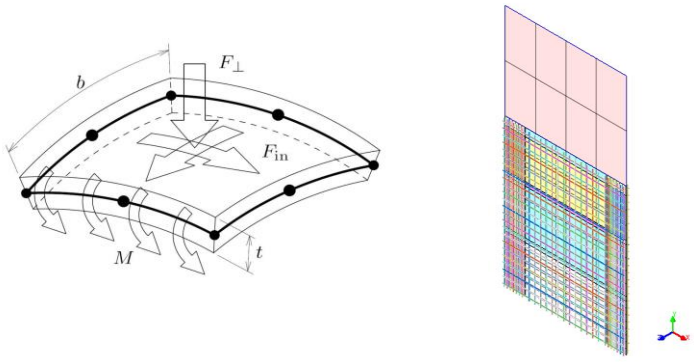

a) b)

Figure 4. Finite Element Model: a) Curved shell element b) A wall model (DIANA 2011)

2.1 **Concrete**

The Total Strain Crack Model available in DIANA (DIANA 2011) is used to represent the behaviour of the concrete elements. The constitutive model based on total strain is developed along the lines of the Modified Compression Field Theory, originally proposed by Vecchio & Collins (1986). As per the multi-directional fixed crack model the total strain based crack models follow a smeared approach for the fracture energy. One of the main advantages of this model over the other concrete models in DIANA is that basic properties can be derived from Model Code regulations for concrete, or they may be input directly. By default, DIANA assumes appropriate values for the various parameters describing the constitutive behavior.

The axial stress-strain data captured using Popovics/Mander`s constitutive model (Mander et al. 1988) (Figure 5a) was implemented in the Total Strain Rotating Crack model to incorporate the confined concrete properties in the boundary elements and behavior of the unconfined portion was modeled using the axial stress-strain relationship of unconfined concrete.

2.2 **Reinforcement**

The reinforcing bars are modelled using Embedded Reinforcement approach available in the program (DIANA 2011). In this approach, reinforcement elements are embedded in structural elements, the so-called mother elements. DIANA ignores the space occupied by the embedded reinforcing bars. The mother element neither diminishes in stiffness, nor in weight. The reinforcement does not contribute to the weight (mass) of the element. Standard reinforcements do not have degrees of freedom of their own. In standard reinforcement the strains are computed from the displacement field of the mother elements. This implies perfect bond between the reinforcement and the surrounding material. The stress-strain curve of the reinforcing steel was defined using Menegotto and Pinto (1973) model (Figure 5b). Bar buckling is not included in this constitutive model, hence the effect of bar buckling is neglected in the analysis.

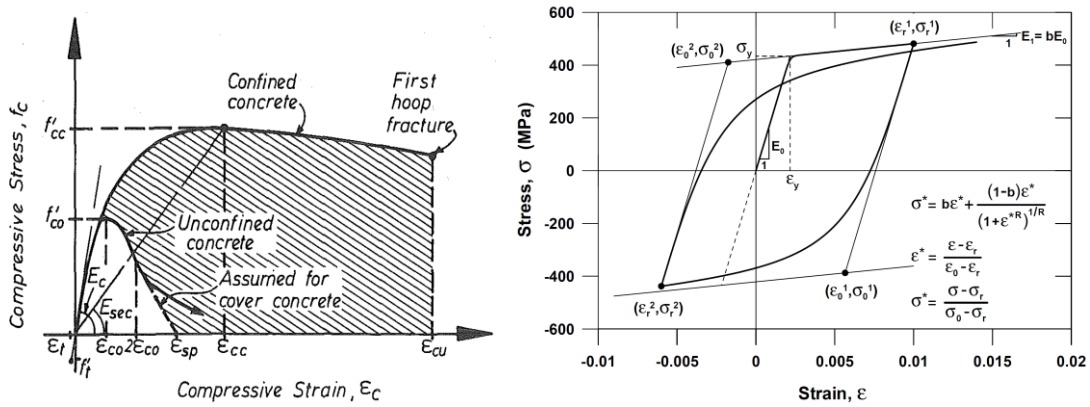

a) Concrete b) Steel

Figure 5. Constitutive models of materials

3 EXPERIMENTAL VERIFICATION

The model is used in the analysis of a number of tested wall specimens with different shear-span ratios. The properties of the specimens chosen for comparison are presented in Table 1. The specimens are chosen based on their shear-span ratios and observed failure modes to evaluate capability of the analysis model in predicting different failure modes. Geometry and reinforcement details of the specimens are shown in Figure 6.

Table 1. Test specimens used for model verification

Specimen	L_w, mm	H_w, mm	t_w, mm	l_b, mm	M/(Vl)	f_c', MPa	Axial Load, kN [Axial Load Ratio]	Failure Pattern
SW11 (Lefas et al. 1990)	750	750	70	140	1.0	42	0 [0.0]	Shear
SW12 (Lefas et al. 1990)	750	750	70	140	1.0	42	230 [0.1]	Shear
SW5 (Vallenas et al. 1979)	2412	3009	114	279	1.6	33.47	598 [0.06]	Flexure - Shear
PW4 (Birely 2013)	3048	3658	152.4	508	2.0	29.5	1601 [0.12]	Flexure – Out of plane
R2 (Oesterle 1976)	1905	4572	101.6	187.3	2.4	46.4	0 [0]	Flexure - Out of plane
RW2 (Thomsen IV and Wallace 1995)	1219	3660	102	172	3.0	42.8	533 [0.1]	Flexure

L_w = length of wall; H_w = height of wall; t_w = web thickness;
l_b = boundary length; M/(Vl) = shear-span ratio.

The base shear-top displacement responses of the specimens are compared with the corresponding test results in Figure 7. The key milestones of a wall response are indicated in Figure 7 with the corresponding values of the lateral load compared with test results in Table 2. The sequence of cracking and yielding in walls with different failure patterns can be tracked using the milestones defined in Table 2 and Table 3. Figure 8 displays the von Mises stress distribution and failure pattern of the specimens. In order to display stress contours in a model like this, it is most appropriate to use the equivalent Von Mises stresses as these represent a scalar value, i.e., without an orientation. As shown in Figure 8, the Von Mises stress values are all positive as the equivalent Von Mises stress is calculated as the square root of a combination of the primary stresses in each element.

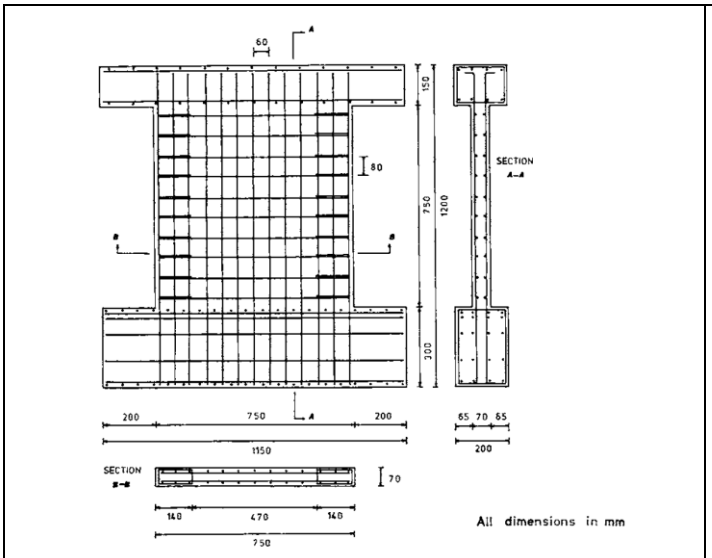

SW11 (Lefas et al. 1990)

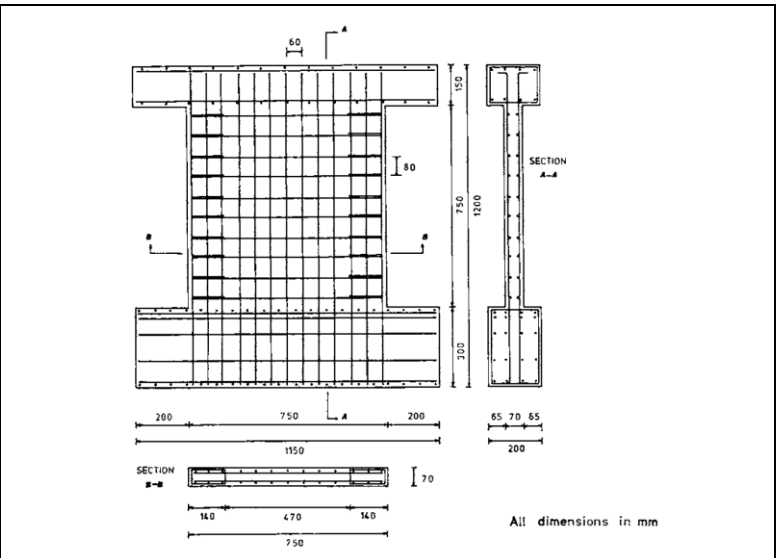

SW12 (Lefas et al. 1990)

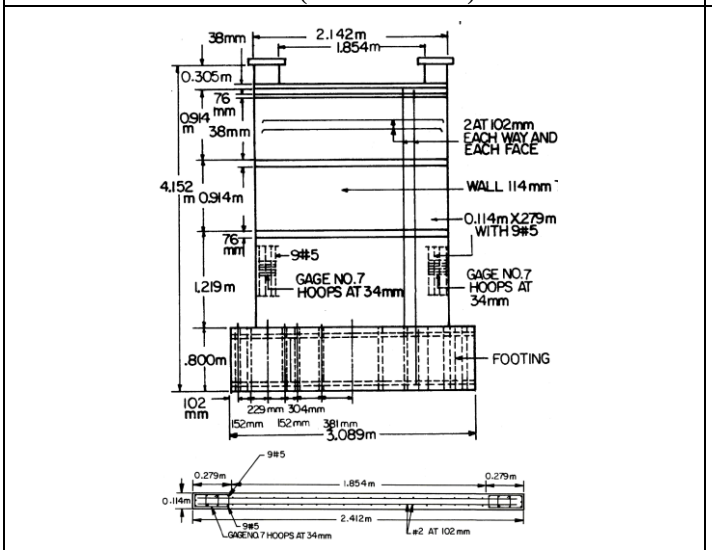

SW5 (Vallenas et al. 1979)

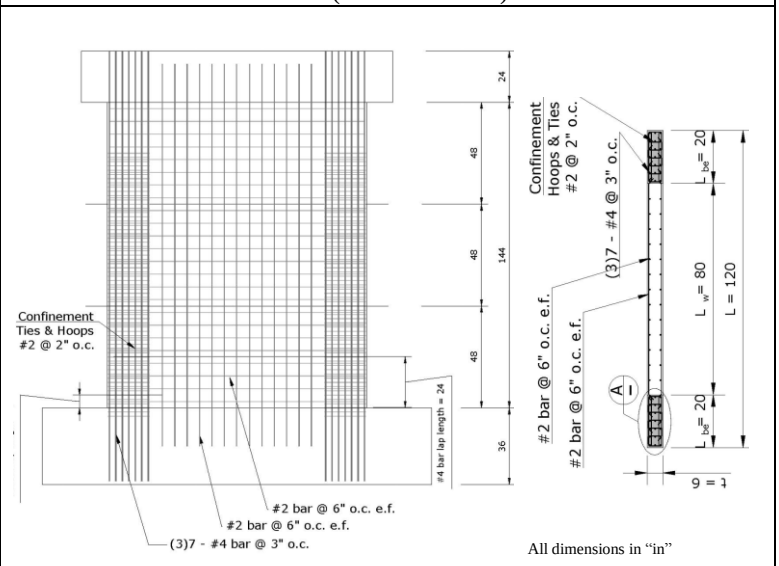

PW4 (Birely 2013)

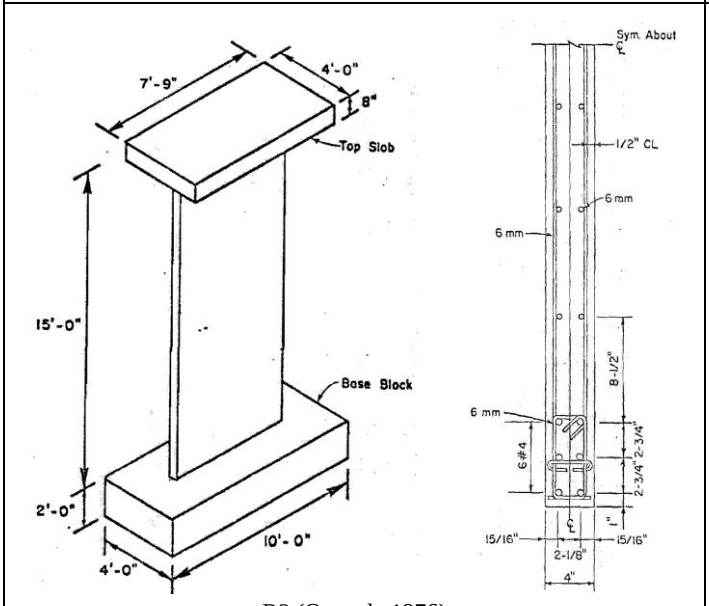

R2 (Oesterle 1976)

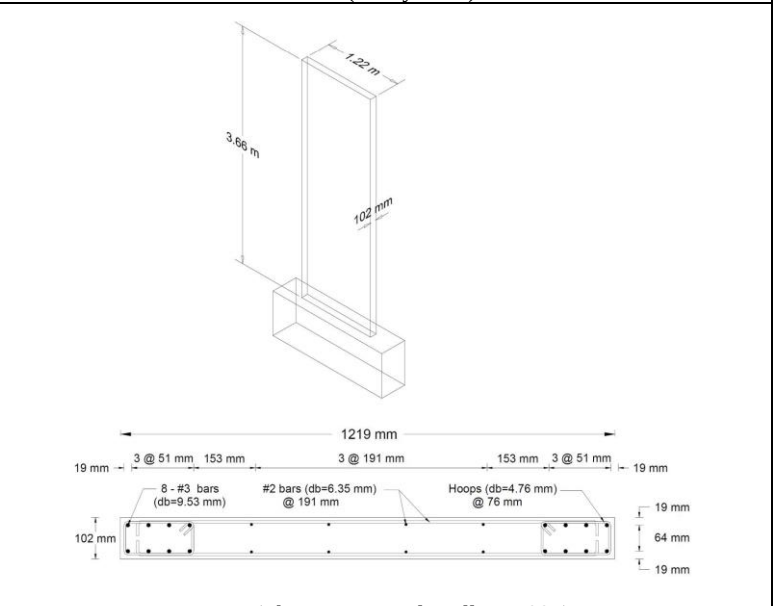

RW2 (Thomsen IV and Wallace 1995)

Figure 6. Geometry and reinforcement details of the specimens

The stress distribution is displayed at 2.5% drift for all the specimens except for Specimen PW4 which failed with considerable out of plane deformation while reversing from the maximum top displacement and reaching zero displacement.

Table 2. Lateral loads corresponding to the key milestones (kN)

Specimen	A: Initiation of Flexural Cracking		B: Initiation of Inclined Cracking		C: First Yield of Tension Reinforcement		D: Tension Yielding of All Boundary Element Reinforcement		E: Initiation of Concrete Crushing at the Base		F: Concrete Spalling Throughout the Boundary Element	
	Test	Analysis	Test	Analysis	Test	Analysis	Test	Analysis	Test	Analysis	Test	Analysis
SW11	35	30.5	100	73.1	170	171.3	-----	209	-----	138	260	232.6
SW12	45	65	130	108	210	241	-----	277	-----	167	340	309
SW5	110	138	250	342	709	533	788	890	840	890	916	903.3
PW4	320	206	380	270	628	575	870	894	870	969	-----	-----
R2	66.7	51.2	-----	94.2	164.6	121	186	132	215	189.8	-----	-----
RW2	74	55	127	97	127	89.7	-----	107.5	138	143	-----	-----

Table 3. Drift values corresponding to the key milestones (%)

Specimen	A: Initiation of Flexural Cracking		B: Initiation of Inclined Cracking		C: First Yield of Tension Reinforcement		D: Tension Yielding of All Boundary Element Reinforcement		E: Initiation of Concrete Crushing at the Base		F: Concrete Spalling Throughout the Boundary Element	
	Test	Analysis	Test	Analysis	Test	Analysis	Test	Analysis	Test	Analysis	Test	Analysis
SW11	0.05	0.01	0.24	0.09	0.48	0.45	-----	0.60	-----	0.36	1.1	0.71
SW12	0.03	0.03	0.17	0.08	0.39	0.45	-----	0.68	-----	0.21	1.18	0.93
SW5	0.07	0.04	0.15	0.08	0.39	0.23	0.42	0.48	0.49	0.48	2.45	1.22
PW4	0.06	0.02	0.07	0.04	0.21	0.18	0.35	0.40	0.5	0.52	-----	-----
R2	0.06	0.03	-----	0.14	0.33	0.2	0.47	0.28	1.11	0.83	-----	-----
RW2	0.18	0.06	0.44	0.2	0.44	0.16	-----	0.27	0.8	0.6	-----	-----

3.1 **Specimens SW11 and SW12**

Specimens SW11 and SW12 were tested by Lefas et al. (1990). These specimens were squat walls (h/l = 1) and were different only in axial load ratio (Table 1). The specimens were subjected to monotonic loading only. Because of its small shear-span ratios (Table 1), response of these two specimens was shear dominated. Figure 7 displays the regular abrupt strength drop of the specimens due to shear failure of the elements happening one after another resulting in brittle response of the specimens. This phenomenon is exacerbated by the axial load applied to Specimen SW12. The experimental measurements are reported up to 1.07% and 1.18% drift for SW11 and SW12, respectively. The analytical predictions show a reasonable match with test results in both specimens. However, the ultimate strength is underestimated for Specimen SW12 which can be attributed to the fact that reinforcement elements are completely dependent on the concrete elements and crushing of a concrete element in this specimen which is considerably contributed by the axial load ratio of 0.1 applied to the specimen is accompanied by complete collapse of the corresponding reinforcement element. In other words, as a concrete element crushes, no additional strength is provided by the corresponding reinforcement element. According to Figure 7, Point E which corresponds to initiation of concrete crushing at the base precedes reinforcement yielding (Table 2) resulting in brittle response of the walls. Von Mises stress distribution of Specimens SW11 and SW12 shown in Figure 8 displays the strut action developed along diagonal of the squat walls indicating shear dominated failure of the specimens. Actually, the stress values

in light coloured area along the walls diagonal is around ten times greater than the ones in the dark coloured area in the stress distribution (Figure 8) indicating that the main load carrying capacity of these walls comes from the diagonal strut action. This stress flow shows orientation of the cracks forming perpendicular to the light coloured strut representing shear cracks observed during the test.

3.2 **Specimen SW5**

Specimen SW5 was a three-story wall specimen tested by Vallenas et al. (1979) and was intended to idealize the three lower stories of a rectangular wall designed for a seven-story prototype building. The specimen was subjected to cyclic loading. As shown in Figure 7, the analytical results are in good agreement with the experimental measurements except that the sudden drop before reaching the maximum top displacement of 80.73mm was not captured by the analysis. According to the test report (Vallenas et al. 1979), the sudden drop was due to the out-of-plane instability of the specimen at compression boundary zone. It should be noted that this specimen was tested in a horizontal position which might have resulted in a loading eccentricity triggering the out-of-plane deformation. The Von Mises stress distribution shown in Figure 8 indicates the contribution of web and compression boundary element in lateral load resistance of the specimen. Actually, as the shear-span ratio of the specimen is greater than 1 (Table 1), its response is governed by both flexure and shear and obviously the shear-flexure interaction which is clearly shown by the ratio of stresses in different areas. Concrete crushing (Point E) started as soon as all the reinforcement in the tension boundary element reached yielding (Point D), which can be attributed to the shear-flexure interaction effect causing initiation of the brittle shear response at the overall yielding of the specimen. This phenomenon is further verified by sequence of the events observed during the test (Table 2 & Table 3).

3.3 **Specimen PW4**

Specimen PW4 was tested by Birely (2013) to address seismic performance of slender reinforced concrete structural walls. Throughout the test, the ratio of the lateral force to the overturning moment applied to the top was held constant such that the base reactions (base shear and base moment; measured at the wall-foundation interface) were equivalent to those of a 10-story wall with a uniform lateral load distribution. In order to generate this effect in analysis, the lateral displacement was applied through an elastic part added at the top of the wall model with a height such that results in a moment at the base corresponding to the top displacement. This way, the ratio of the lateral force to the overturning moment could be held constant. In other words, the base moment and shear applied during the test was applied in the analysis by increasing the height of the model. According to Figure 7, the cyclic response of the specimen was well captured by the analysis. A considerable drop of strength observed in the experimental response is corresponding to specimen failure which had occurred due to extensive bar buckling and core crushing as well as out of plane movement in the east (right) boundary element at the toe of the wall during the second cycle of 1.0% drift. Since bar buckling was not taken into account in the analysis the analytical model did not lose the load carrying capacity and 1 more cycle of 1.5% drift was applied to the model. Out of plane deformation was observed as the model reached zero displacement after +1.5% drift. The shear-span ratio of this specimen (Table 1) is low enough to cause the shear actions to affect the wall response to some extent. According to test results (Table 2 & Table 3), concrete crushing (Point E) was simultaneous with tension yielding of all boundary element reinforcement (Point D). The analysis prediction of Points D and E was also very close-by.

3.4 **Specimen R2**

Specimen R2 is one of the specimens tested by Oesterle (1976) at Portland Cement Association Laboratories. According to the test report, considerable out of plane deformation was observed during the test. The analysis did not converge during the final cycle since a considerable out of plane deformation resulted in instability of the wall model. The analysis could reasonably predict the base shear-top displacement response of the specimen until instability of the model due to out of plane deformation at the compression boundary element (Figure 7).With a shear-span ratio of 2.4 (Table 1), response of this specimen was flexure dominated with out of plane failure (Figure 8).

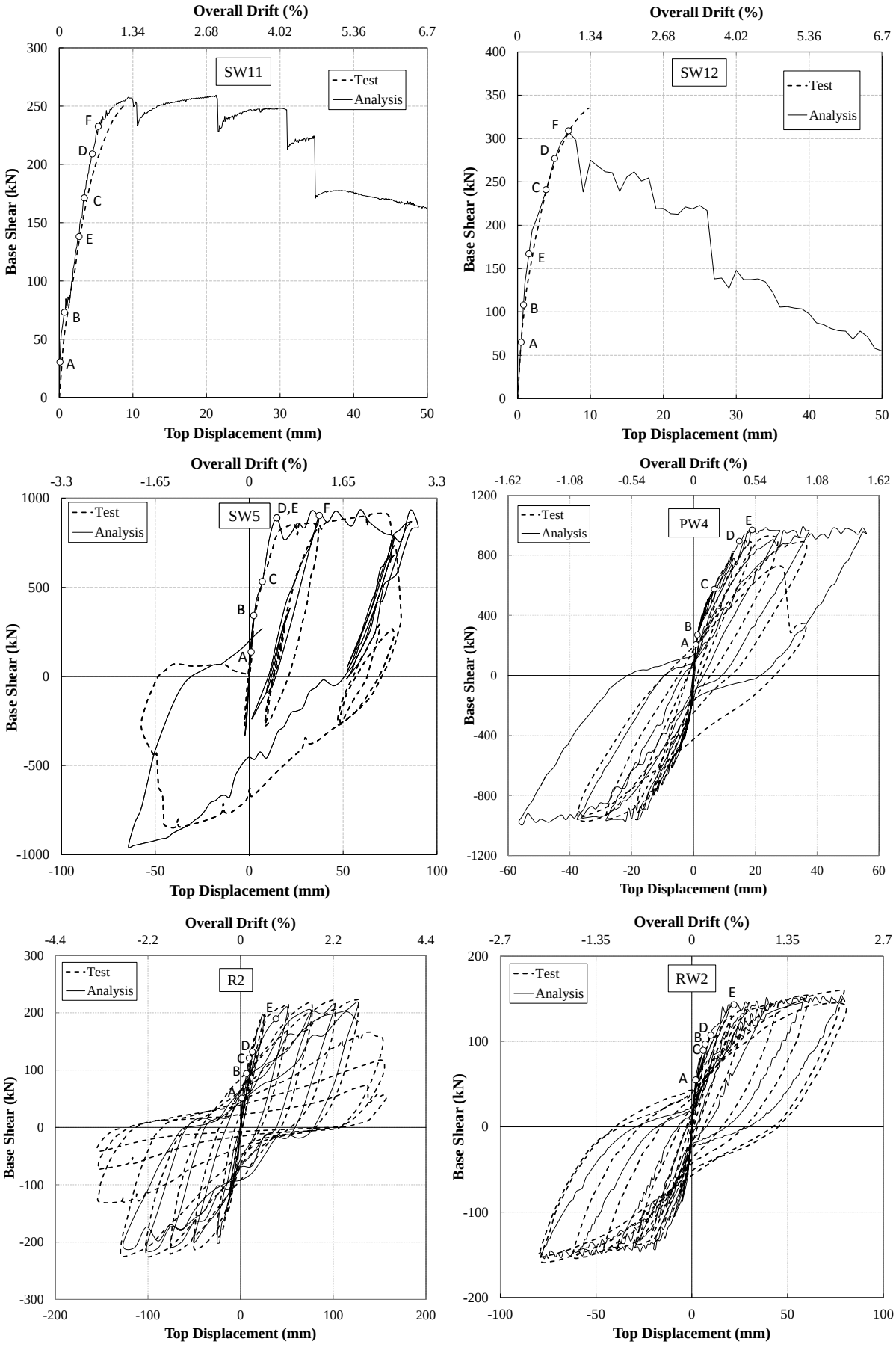

Figure 7. Base shear-top displacement response of the specimens (See Table 2 for definition of Points A-F)

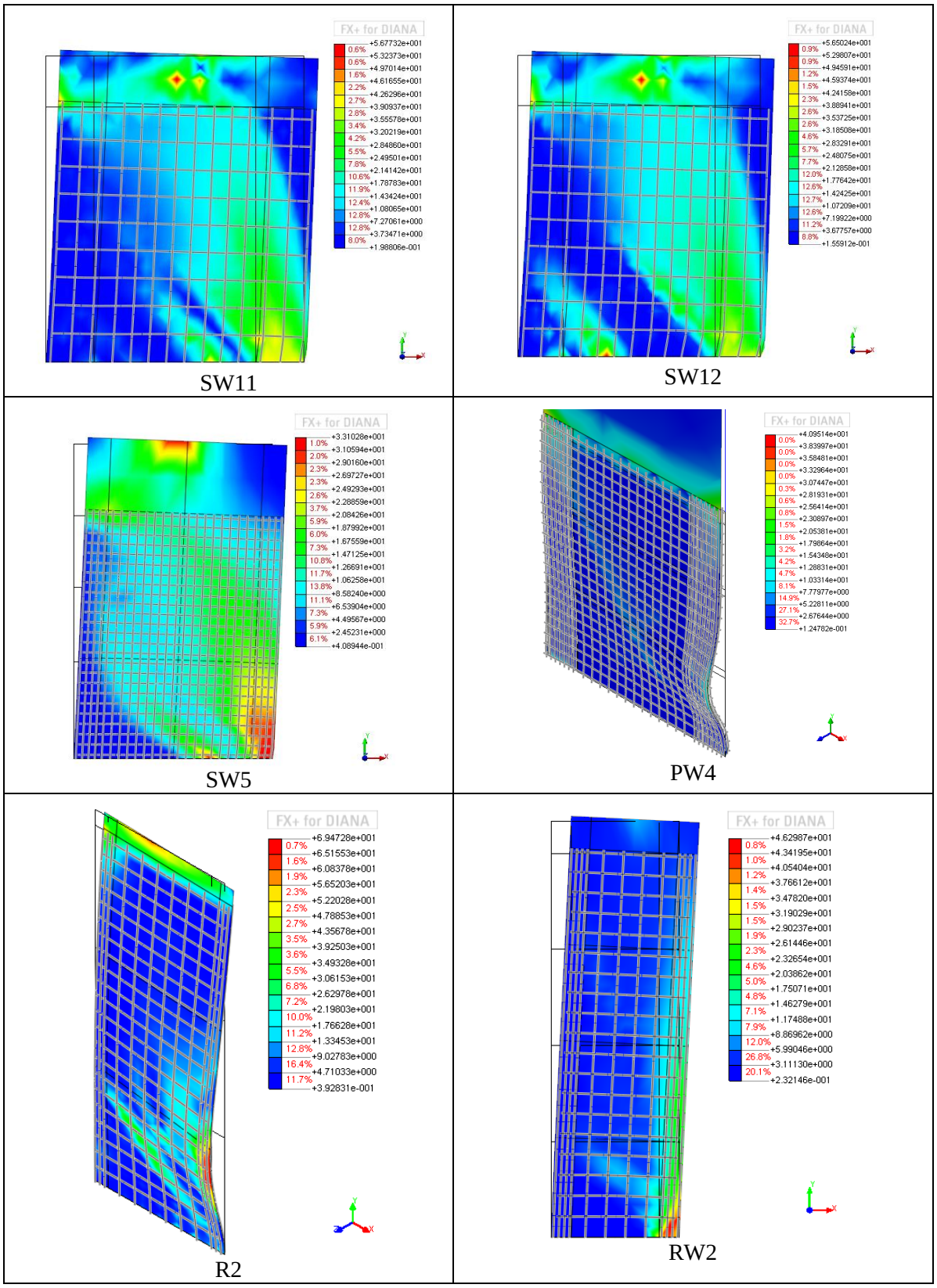

Figure 8. Von Mises stress distribution and failure pattern of the specimens

3.5 **Specimen RW2**

Specimen RW2 was tested by Thomsen IV and Wallace (1995). A constant axial load of approximately 0.1Agf`c was applied to the wall prior to application of the displacement controlled lateral load history. The specimen failed due to bar buckling at 2.5% drift. With a shear-span ratio of 3, response of this specimen was flexure dominated. Figure 7 shows a reasonable match between analytical and experimental hysteresis curves. The Von-Mises stress distribution (Figure 8) clearly shows that the main contribution to the lateral load resistance of the wall comes from boundary elements and flexure is dominant in this specimen as the stress values in the compression boundary element are about ten times greater than the stress values in the panel. Therefore, the load carrying capacity of the wall mainly comes from the concrete in the compression boundary element and reinforcement in the tension boundary element (which is not shown in Figure 8) resulting in flexure dominated response of the model.

Figure 9 displays the concrete strain measurements of Specimen RW2 at wall base in comparison with the model predictions at the positive peak of selected drift cycles applied during testing. The average concrete strains were measured by seven LVDTs over a 229 mm gage length at the base of the wall. The average concrete strain of two consecutive meshes (100x100mm) at the base is used for comparison. As shown in Figure 9, the analysis could reasonably predict the strain profile at different drift levels. At the 2% drift level the difference between the test and analysis is relatively more although the strain profiles follow the same pattern. The difference at the 2% drift level can be attributed to the bond-slip effect which becomes more influential at higher displacement levels and is not considered in the analysis. Also, the neutral axis position which is one of the main factors in calculating confinement length is well predicted by the analysis.

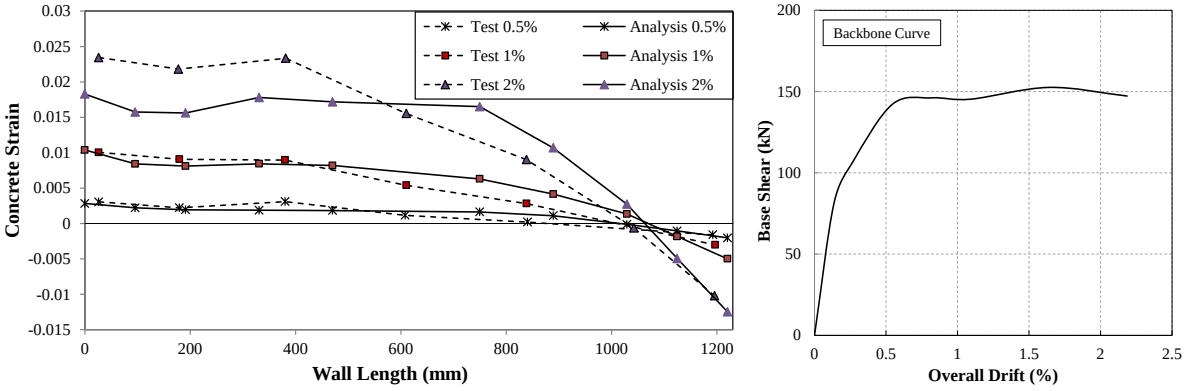

Figure 9. Wall strain gradient, Specimen RW2

4 **CONCLUDING REMARKS**

Validity of a finite element modelling and analysis approach was evaluated using test results of six wall specimens with different shear-span ratios and failure patterns. Curved shell elements with embedded bar elements were used to simulate reinforced concrete walls in a commercial FE analysis program DIANA. The model predictions were in reasonably good agreement with the experimental measurements for all specimens. Specimen SW11 was a squat wall and was shear dominated. Specimen SW12 had the same properties as SW11 except that an axial load ratio of 0.1 was applied to the specimen. The axial load affected the base shear-top displacement curve resulting in a more brittle response. Specimen SW5 had a flexure-shear failure pattern as its shear-span ratio was such that both flexure and shear contributed to the wall response. The analysis could not predict the out-of-plane deformation that was observed during the test. The specimen was tested in a horizontal position which could have triggered the out-of-plane instability. Specimen PW4 with a flexure dominated response had out-of-plane deformation during the test which contributed to the instability of the specimen at the final stages of loading. The model could predict this type of deformation. Out of plane deformation was observed during the test procedure in Specimen R2 and was well captured by the model. This

specimen was a slender rectangular wall with a flexure dominated response. Specimen RW2 had the greatest shear-span ratio among the selected specimens resulting in the response being flexure dominated. The model predictions matched well with experimental measurements for this specimen in terms of lateral load-top displacement response as well as the strain gradient at the base indicating that in addition to the overall global response predictions, local behaviour of the wall models can also be predicted reasonably well. The sequence of events observed during the tests and predicted by the analysis showed initiation of concrete spalling before initiation of reinforcement yielding for squat walls which had brittle shear failure and very close-by occurrence of concrete crushing and overall yielding for specimens with shear-flexure failure.

The FEM analysis could simulate the nonlinear response and failure pattern of specimens with different failure modes and can be used as a tool to comprehensively scrutinize the main factors governing different failure patterns including the out of plane instability which, in the authors' knowledge, has not yet been predicted analytically by other researchers.

REFERENCES

Birely, A. C. 2013. Seismic Performance of Slender Reinforced Concrete Structural Walls, University of Washington. PhD: 983.

DIANA, T. 2011. Finite Element Analysis User's Manual - Release 9.4.4, TNO DIANA.

Elwood, K. J. 2013. Performance of concrete buildings in the 22 February 2011 Christchurch earthquake and implications for Canadian codes 1, Canadian Journal of Civil Engineering, 40(3): 1-18.

Kam, W. Y., S. Pampanin and K. Elwood. 2011. Seismic performance of reinforced concrete buildings in the 22 February Christchurch (Lyttelton) earthquake, Bulletin of the New Zealand Society for Earthquake Engineering, 44(4): 239-278.

Lefas, I. D., M. D. Kotsovos and N. N. Ambraseys. 1990. Behavior of reinforced concrete structural walls: strength, deformation characteristics, and failure mechanism, ACI Structural Journal, 87(1).

Mander, J., M. N. Priestley and R. Park. 1988. Theoretical stress-strain model for confined concrete, Journal of structural engineering, 114(8): 1804-1826.

Menegotto, M. and P. Pinto. 1973. Method of Analysis for Cyclically Loaded Reinforced Concrete Plane Frames Including Changes in Geometry and Non-elastic Behavior of Elements Under Combined Normal Force and Bending. IABSE Symposium on the Resistance and Ultimate Deformability of Structures Acted on by Well-Defined Repeated Loads, Lisbon.

NZRC. 2012. Canterbury Earthquakes Royal Commission Reports, http://canterbury.royalcommission.govt.nz /Final-Report-Volume-Two-Contents.

Oesterle, R. 1976. Earthquake Resistant Structural Walls: Tests of Isolated Walls, Research and Development Construction Technology Laboratories, Portland Cement Association.

Park, J. and Y. Chen. 2012. Understanding and Improving the Seismic Design of Shear Walls. Final Year Projects, Dept. of Civil and Natural Resources Engineering, University of Canterbury.

Thomsen IV, J. H. and J. W. Wallace. 1995. Displacement-based design of reinforced concrete structural walls: An experimental investigation of walls with rectangular and T-shaped cross-sections. Report No. CU/CEE-95-06, Department of Civil and Environmental Engineering, Clarkson University, Potsdam, N.Y.

Vallenas, J. M., V. V. Bertero and E. P. Popov. 1979. Hysteretic behaviour of reinforced concrete structural walls. Report no. UCB/EERC-79/20, Earthquake Engineering Research Center, University of California, Berkeley.

Vecchio, F. J. and M. P. Collins. 1986. The modified compression-field theory for reinforced concrete elements subjected to shear, ACI J., 83(2): 219-231.